CHAPTER VI

SYNTHESIS AND ELECTRICAL PROPERTY STUDY OF $La_3Ni_2MO_9$ (M = Nb AND Ta)

6.1 Abstract

Synthesis of $La_3Ni_2NbO_9$ and $La_3Ni_2TaO_9$ double perovskite materials were successfully carried out both by the solid state reaction and sol-gel processes. Crystal structures of the compound have been studied using XRD analysis. Both isostructural niobates and tantalates exhibited the monoclinic space group $P2_1/n(14)$. The solid state reaction yielded the single phase only in $La_3Ni_2NbO_9$, while the higher purities were obtained by the sol-gel process. $La_3Ni_2NbO_9$ has more possible ordered arrangements than $La_3Ni_2TaO_9$. Nb and Ta substitution in $La_3Ni_2MO_9$ had effect on the sintering behavior which caused the clear grain boundary of $La_3Ni_2TaO_9$ more than $La_3Ni_2NbO_9$. The electrical conductivities of $La_3Ni_2NbO_9$ were found to significantly increase with increase of temperature. But the electrical conductivities of $La_3Ni_2TaO_9$ decreased with temperatures when the temperature is lower than 300°C then slightly increased again at higher temperature.

(**Keywords**: Cathode, Solid oxide fuel cell, Double perovskite)

6.2 Introduction

Solid oxide fuel cells (SOFCs) are believed to be promising as generation power systems with their high energy conversion efficiency, environmental compatibility, and ability to use hydrocarbon fuels directly without external reforming. However, the Achilles'heel of SOFC is due to its high operating temperature leading to short term stability and high component costs. It has been desirable in the research community to reduce the operating temperature to intermediate at 400-600°C (IT-SOFCs) while still maintaining high efficiency as high temperature. New electrode and electrolyte materials have been investigated to achieve such operating temperature target [1-4].

Oxides with perovskite structures have been used in and studied for many applications including magnetoresistance, superconductor, ferroelectric, piezoelectric, magnetic and ion conducting applications. Perovskite structures with the general formula $ABO_3$are highly flexible which almost all elements in the periodic table can be accommodated on the A and/or B sites [2]. Perovskite compounds such as Sr doped lanthanum iron cobalt oxide (LSCF) have been identified as potential cathodes for IT-SOFC [5-7]. They exhibit very good conductivity, but exhibit large thermal expansion mismatch with the other cell components, causing thermomechanical failure [4].

Materials with Ruddlesden-Popper structure (A_2BO_4) which is comprised of alternating perovskite blocks with a rock-salt intergrowth have been attractive due to their mixed conducting properties while maintaining high electrical conductivity in the targeted temperature range [8–11]. These materials, particularly the nickelate series ($La_{n+1}Ni_nO_{3n+1}$), have caught much attentions because of the relatively open structural framework supported by the rock-salt intergrowth in its structure. Such an opened structure allows excess oxide-ions to be accommodated in the rock-salt layer resulting in improvements in ion conductivity [12-13]. La_2NiO_4 (n = 1) is a mixed ionic and electronic conductor with high oxygen diffusivity due to its high oxygen vacancy concentration [8-9, 14]. In addition, the higher-order Ruddlesden-Popper phases (n > 1, $La_3Ni_2O_7$ and $La_4Ni_3O_{10}$) were found to exhibit good long-term stability, and thus they are potentially more suitable than the n = 1 compound in solid

oxide fuel cell (SOFC) devices [12]. However, the higher–order RP phases ($n > 1$) have been found to be difficult to synthesize directly, lengthy processing times (4-5 days) and are energy intensive [15-16].

Because of almost all elements in the periodic table can be accommodated on the A and/or B sites, perovskite structures with the general formula ABO_3 are highly useful structures. [2,17]. If two atoms, B and B′, are placed on the two crystallographic different B-sites, a layered perovskite is formed with the general formula $A_2BB'O_6$. B and B′ can be completely or partially ordered depending on the size and charge differences between the B ions and the degree of ordering also strongly affected on the properties of these materials.

One variation of pervoskite structure is a double perovskite with the general formulation $A_3B_2B'O_9$ when the B and B′ ratio is 2:1 [17]. Such structure could have the ordering in a rock salt pattern with different cations occupying alternating BO_6 octahedra. The B-site ordered perovskites should be similar to the relatively open structural framework as Ruddlesden-Popper structure which allows for the accommodation of hyper-stoichiometric oxide-ions in the rock-salt layer resulting improvement of ion conductivity. Because of its wide range of properties, the double perovskites is interesting to be the new candidate of IT-SOFC cathode [17-19].

Recently, Kim *et al.* studied a family of double perovskite oxides, $NdBa_{1-x}Sr_xCo_2O_{5+\delta}$ (x = 0 and 0.5) [20]. They found that the substitution of Co by Ni in $GdBaCo_{2-x}Ni_xO_{5+\delta}$ leads to slightly improved performance in SOFC with an important advantage of lower TEC because the TEC value decreases with increasing Ni content and reaches 16.7×10^{-6} K^{-1} for the x = 0.6, which is ~13% lower than the TEC of the x = 0 sample. Moreover, Hu *et al.* successfully synthesized $GdBaCo_{2-x}Ni_xO_{5+\delta}$ (x = 0-0.8) synthesized by a citrate-gel modified chemical route, by which we have achieved a high level of substitution up to $x = 0.8$ and resulted that the TEC value was also reduced [21]. Although the electrical conductivity decreases with increasing Ni content, all Ni compositions still show conductivity more than 300 S/cm up to 900°C, which is adequate for employing them as cathodes in SOFC [20]. Not only the electrical conductivity which is significant property of SOFC cathode, but the ionic conductivity is also concerned. Tao *et al.* reported in 2002 that in

perovskites with the formulation $A_3B_2B'O_{9-\delta}$, when B′ was the valance +5 elements such as Nb and Ta, could exhibit high proton and oxygen ion conductivity [12]. So, the improvement of ionic conductivity should be found in the B-site ordered perovskites. However, there are still very few reports on the electrical conductivity in the double perovskites with the formulation $A_3B_2B'O_{9-\delta}$, particularly with B-site as Nb and Ta substitution on Ni, while the ionic transport property seems to never study before. In this work, we studied the synthesis and characterization of the new triple perovskites family: $La_3Ni_2MO_9$ with M = Nb or Ta. These new compounds have been synthesized simply by both solid–state reaction and sol-gel process. The effects of synthesis routes and B–site dopants (Nb and Ta) on phase and morphology were examined, while the electrical conductivity was investigated as the primary result.

6.3 Experimental

6.3.1 Preparation of $La_3Ni_2MO_9$

6.3.1.1 Solid State Reaction

$La_3Ni_2MO_9$ (M = Nb and Ta) compounds were prepared by adding the stoichiometric amounts of Lanthanum oxide (La_2O_3, 99.9%, REacton®), Nickel oxide (NiO, 99%, Alfa Aesar) and Niobium (V) oxide (Nb_2O_5, 99.5%, Alfa Aesar) and tantalum (V) oxide (Ta_2O_5, 99%, Hopkin & Williams Ltd.) into a polypropylene bottle filled with ZrO_2 balls. The mixture was ball milled for 24 hr. The powder was, afterwards. ground and calcined at 1400°C with the heating rate 300°C/hr for 24 hrs in air.

6.3.1.2 Sol-Gel Process

Synthesis of $La_3Ni_2NbO_9$: The first precursor solution was prepared using lanthanum acetate ($(CH_3COO)_3La{\bullet}1.5H_2O$, 99.9%, Alfa Aesar) and nickel acetate ($(CH_3COO)_2Ni{\bullet}4H_2O$, 98+%, Alfa Aesar). The two compounds were stoichiometrically mixed and were dissolved in acetic acid (99.7+%, ACS, Alfa Aesar). Deionized water was added afterwards and the solution was stirred and heated up to 80°C until a clear green solution was obtained. The second precursor solution was prepared in a separated beaker. Citric acid ($HOCOCH_2C(OH)(COOH)$

CH_2COOH, 99.5%, anhydrous, Alfa Aesar) was dissolved in 40 ml of water. Niobium (V) oxalate hydrate ($C_{10}H_5NbO_{20}$•xH_2O, ACS, Alfa Aesar) was then added before the mixture was stirred and heated up to 80°C to obtain a white solution. The precursor solutions prepared above were mixed together until homogenous. Additional citric acid and ammonia solution (NH_4OH, 28.0-30.0%, ACS, Alfa Aesar) were added into the mixture afterwards to prevent the precipitation (the solution was clear and blue colour). The mixture was stirred continuously at 80°C until a green gel was formed. The gel was fired at 300°C for 12 hrs with heating rate 5°C /min to obtain dark olive green almost black powder. The resulting powder was ground and then fired again at 600°C for 12 hrs with the heating rate of 5°C/min to remove organic components. The calcined powder was then ground again and was fired at 1400°C for 24 hr with a heating rate of 5°C/min.

Synthesis of $La_3Ni_2TaO_9$: The first precursor solution was prepared using lanthanum acetate ($(CH_3COO)_3La$•xH_2O, 99.9%, Sigma-Aldrich Co.) and Nickel acetate ($(CH_3COO)_2Ni$•$4H_2O$, 98%, Sigma-Aldrich Co.). The two compounds were stoichiometrically dissolved in the solution of ethylene glycol ($HO–CH_2CH_2–OH$, ≥98%, Sigma-Aldrich Co.) and acetic acid (glacial, 100%, Merck) and stirred until a clear green solution was obtained. The second part of the precursor was prepared by dissolving tantalum (V) ethoxide ($Ta(OC_2H_5)_5$, 99.98%, Sigma-Aldrich Co.) in a solution of 2–methoxyethanol (CH_3OCH_2 CH_2OH, anhydrous, 99.8%, Sigma–Aldrich Co.) and acetic acid (glacial, 100%, Merck). Acetylacetone (≥99%, Merck) was then added followed by heating to 150°C for 30 min and then left to room temperature. To obtain the desired gel, the two precursor solution was mixed heated at 60°C. Triethanolamine ($C_6H_{15}NO_3$, 99%, Merck) was added until the pH was measured to be in the range of 5-6. The mixture was stirred for 15 hrs and the gel was formed. The gel was fired at 300°C for 12 h with heating rate 5°C /min to obtain dark green powder. The powder was ground and fired again at 600°C for 12 h with heating rate 5°C/min to remove the organic solvent and ground and calcined again at 1400°C for 24 h with heating rate 5°C/min.

6.3.2 Characterization

Phase analysis was performed on all samples. The samples were analyzed using a Philips PW 1700 Series x–ray diffractometer with Cu Kα source (λ = 1.5418 Å) over 20-80° 2θ range. Graphite secondary crystal monochromator was used with at a generator of 40 kV and 40 mA. Full profile fitting and refinement was performed to confirm the crystal structure along with the corresponding lattice parameters using JADE 9 X-ray analysis software (MDI, CA, USA). The morphologies were studied by using a JEOL 5610 SEM.

6.3.3 Electrical Conductivity

As prepared powder of $La_3Ni_2NbO_9$ and $La_3Ni_2TaO_9$ was uniaxial pressure at 120 MPa bars followed by isostatic pressing at 300 MPa. The samples were sintered at 1500°C for 24 hrs with a heating rate of 300°C/hr. The sintered samples were cut into 15 mm length and were polished. Pt wire and Pt paste was used as the conducting wire and conductive paste for wire attachment respectively. The curing of the sample before the measurement was done at 800°C for 1 hr with heating rate 300°C/hr. The conductivities of the bar specimens were measured as a function of temperature by using the four-point direct current conductivity technique under static air conditions. The measurements were performed starting from room temperature to 850°C with 50°C measurement intervals with heating rate 300°C/hr. In order to achieve equilibration at each measured temperature, a prolonged dwell time (15 min) was used to ensure stable readings. Conversely, the measurements also were measured starting from 850°C to room temperature with 50°C measurement intervals with cooling rate 300°C/hr.

6.4 Results and Discussion

6.4.1 Phase Formation

Fig. 6.1 shows the XRD patterns of $La_3Ni_2NbO_9$ samples prepared by (a) the solid state reaction and (b) the sol-gel process. The double perovskite structure of the $La_2Mg_{1.33}Nb_{0.67}O_6$ crystal structure (JCPDS 04-014-9726) was taken as the model for $La_3Ni_2NbO_9$ compounds. $La_3Ni_2NbO_9$ could be well described with

the monoclinic space group $P2_1/n(14)$ and was found to be the dominant phase in both samples. $La_3Ni_2NbO_9$ prepared by the solid state reaction was identified to be a single phase, while some impurity phases such as La_2O_3 (2θ = 27.94°) could be detected in $La_3Ni_2NbO_9$ samples prepared by the sol-gel process. Fig. 6.2 shows XRD patterns of the $La_3Ni_2TaO_9$ samples prepared by (a) solid state reaction and (b) sol-gel process. In the case of $La_3Ni_2TaO_9$ prepared by solid state reaction, the double perovskite phase was also identified with the monoclinic space group $P2_1/n(14)$, while the minor phases appeared to be La_2O_3 with XRD peaks at 2θ = 28.45 and 29.95°, and NiO at 2θ = 43.33°. Even though, the double perovskite $La_3Ni_2TaO_9$ structure prepared by sol-gel process also was identified same as in prepared by solid state reaction, the minor phase was found to be different. La_3TaO_7 was found at 2θ = 27.99°, 28.33°, 32.93°, 46.59°, 55.63° and 56.22° (JCPDS 04-010-0643), while La_2O_3 and NiO were almost undetectable.

Because of almost undetectable of impurities in $La_3Ni_2NbO_9$, this can imply that $La_3Ni_2NbO_9$ compound shows the possible ordered arrangement more than $La_3Ni_2TaO_9$, especially as shown the single phase of $La_3Ni_2NbO_9$ double perovskite as shown in Fig. 6.1(a). An ionic radius of Nb^{5+} (0.64 Å) is almost the same as that of Ta^{5+} (0.64 Å) resulting in the presence of isostructural niobates and tantalates [23], but there are the slight differences in the phase formation of Nb^{5+} and Ta^{5+} dopants. In 2004, Lufaso studied the crystal structures of 2:1 ordered $Ba_3MM'_2O_9$ (M = Mg, Ni, Zn; M′ = Nb, Ta) perovskites [24]. He indicated that the bond valence sums calculated from the bond distances indicate Ba–O bonds are compressed, while the M–O and $M'–O_6$ bonds are expanded from ideal lengths caused by a shift of Ta^{5+} and Nb^{5+} out of center of the $[M'O_6]$ octahedral. The octahedral distortion is driven by the asymmetry in the O bonding network and aided by the second-order Jahn-Teller distortion of the d^0 of Nb^{5+} and Ta^{5+} cations. These can be explained the slight differences in covalent bonding between Nb^{5+} and Ta^{5+} in which Nb^{5+} is expected to be higher the degree of overlap between the low lying empty d orbitals and the filled O 2p orbitals than Ta^{5+}. Such overlap is the reason for Nb^{5+} to be more covalent than Ta^{5+}. Thus, Nb^{5+} has a higher preference for occupying a more distorted coordination environment, while Ta^{5+} typically

crystallizes with a more symmetric coordination environment [24]. These may be the reason why $La_3Ni_2NbO_9$ compound shows the more possible ordered arrangement than $La_3Ni_2TaO_9$.

Comparing between the two synthesized methods, it was found that the samples synthesized via the sol-gel process have a small difference in slightly more detectable impurity phases than the samples synthesized via the solid state reaction. La_2O_3, NiO and La_3TaO_7 were found in the samples produced via the sol-gel process, while the impurity phases are almost undetectable in the samples synthesized by the solid state reaction. This may be due to the higher ordered materials generally proceed via the initial formation of intermediate phases which then undergo further reactions and the sol-gel process involves several reactions which is more difficult to control than the solid state reaction [15]. Therefore, the samples synthesizes by solid state reaction were chosen to further characterization.

6.4.2 Morphological Observation

Fig. 6.3 shows SEM images of $La_3Ni_2MO_9$ powder (M = Nb and Ta) prepared by the solid state method after being fired at 1400°C for 24 h. For the $La_3Ni_2NbO_9$ samples, slightly smaller particle size was observed (left) comparing to the $La_3Ni_2TaO_9$ samples (right), $La_3Ni_2TaO_9$ particles exhibit a less facetted particle morphology than the $La_3Ni_2NbO_9$ samples. Moreover, adding of Nb and Ta in $La_3Ni_2MO_9$ is not only influence on the phases, but also exhibits an impact on the microstructure, especially in sintering behavior. Fig. 6.4 shows the SEM images at different magnifications of $La_3Ni_2MO_9$ powder (M = Nb and Ta) prepared by the solid state reaction after being sintered at 1500°C for 24 h. The micrographs show the sintered $La_3Ni_2NbO_9$ samples (left) which have less porosity than the sintered $La_3Ni_2TaO_9$ samples (right). Such better sintering characteristics for the Nb substituted samples maybe explained by the lower melting temperature of Nb_2O_5 vs. Ta_2O_5 at 1485°C and 1800°C, respectively [15]. Such lower melting temperature of the oxide could indicate the lower melting point and lower sintering temperature of the Nb substituted compound.

6.4.3 Electrical Conductivity

Fig. 6.5 shows the electrical conductivity results of the sintered $La_3Ni_2MO_9$ (M = Nb and Ta) samples produced by the solid state reaction as a function of temperature in both heated up and cooled down measurements. In the case of $La_3Ni_2TaO_9$, a small hysteresis behavior was observed upon heating and cooling. This was explained by Kammer [26] who proposed that the perovskite phase can re–organize when the perovskite is heated or cooled. However, for $La_3Ni_2NbO_9$, a hysteresis was almost unseen. In addition, it is clearly seen that the electrical conductivities of $La_3Ni_2NbO_9$ significantly increase with increase of temperature. But the electrical conductivities of $La_3Ni_2TaO_9$ decreased with temperatures when the temperature is lower than 300°C then slightly increased again at higher temperature. This is also found by Xu *et al.* [27] who explained that Nb and Ta doping influence the conductivity mainly in following two aspects: one is changing the carrier concentration and the other is introducing scattering centers in conducting plane. At low doping level, the change of carrier concentration dominates the conducting behavior, so a transition from semiconductor to metal takes place. At high doping level, however, the strong scattering may dominate the conducting behavior; thus, a metal–nonmetal transition occurs [27]. That means that the conductivity behaviour of $La_3Ni_2MO_9$ (M = Nb and Ta) depends on the suitable amounts of each dopants. These may be the results that why the conductivities of $La_3Ni_2NbO_9$ are lower than $La_3Ni_2TaO_9$. Moreover, the different conductivities of both compounds may be also explained by Palanduz *et al.* [28] who proposed why $SrBi_2Ta_2O_9$ (SBT) and $SrBi_2Nb_2O_9$ (SBN) behave so differently when Ta^{+5} and Nb^{+5} have very similar chemical behaviors. Because of their structures consist of perovskite-like layers and metal oxide layers, when Ta^{+5} and Nb^{+5} were added, the different layers dominate the conductivity depending on the easier reducibility of Nb^{+5} and Ta^{+5}. Although, the electrical conductivities of $La_3Ni_2NbO_9$ and $La_3Ni_2TaO_9$ are not high enough to be IT-SOFCs cathode, the further studies including the appropriate amounts of Nb and Ta, the thermal stability and ionic conductivity are interesting to understand their materials.

6.5 Conclusions

The synthesis of $La_3Ni_2NbO_9$ and $La_3Ni_2TaO_9$ double perovskite materials was successfully carried out both by the solid state reaction and sol-gel process. The solid state reaction was shown to yield a single phase of $La_3Ni_2NbO_9$, while the higher purities were obtained by the sol-gel process. $La_3Ni_2NbO_9$ has more possible ordered arrangement than $La_3Ni_2TaO_9$ because Nb^{5+} is expected to be higher the degree of overlap between the low lying empty d orbitals and the filled O 2p orbitals than Ta^{5+} resulting Nb^{5+} is more covalent than Ta^{5+}. Thus, Nb^{5+} has a higher preference for occupying a more distorted coordination environment, while Ta^{5+} typically crystallizes with a more symmetric coordination environment. Adding of Nb and Ta in $La_3Ni_2MO_9$ does not only influence on the phases, but also has an impact on the microstructure, especially in sintering behaviour. A hysteresis of electrical conductivity of $La_3Ni_2TaO_9$ was observed on heating and cooling, while $La_3Ni_2NbO_9$ was almost not observed. The electrical conductivities of $La_3Ni_2NbO_9$ significantly increase with increase of temperature. But the electrical conductivities of $La_3Ni_2TaO_9$ decreased with temperatures when the temperature is lower than 300°C then slightly increased again at higher temperature. However, the $La_3Ni_2NbO_9$ and $La_3Ni_2TaO_9$ materials need further improvement because the electrical conductivities are not yet suitable for use as IT-SOFCs cathode.

6.6 Acknowledgements

This work was partially funded by the postgraduate education and research programs in Petroleum and Petrochemical Technology (PPT Consortium), Rachadapisake Sompote fund, Chulalongkorn University, the Development and Promotion of Science and Technology, Thailand project (DPST), and the National Metal and Materials Technology Center (MTEC), Thailand for financial support. I would like to thank Dr. Sumittra Charojrochkul from MTEC, Thailand and staff at the Department of Materials, Imperial College London. This research was also supported by a Marie Curie Intra European Fellowship within the seventh European Community Framework Programme (PIEF-GA-2009-252711).

6.7 References

[1] Minh, N.Q. (1993) Ceramics fuel cells. J. Am. Cerum. Soc., 76 (3), 563-588.

[2] Ormerod, R.M. (2003) Solid oxide fuel cell. Chem. Soc. Rev., 32, 17-28.

[3] Ralph, J.M., Schoeler, A.C., and Krumpelt, M. (2001) Materials for lower temperature solid oxide fuel cells. J. Mater. Sci., 36, 1161-1172.

[4] Chiba, R., Yoshimura, F., and Sakurai, Y. (1999) An investigation of $LaNi_{1-x}Fe_xO_3$ as a cathode material for solid oxide fuel cells. Solid State Ionics, 124, 281-288.

[5] Tai, L.-W., Nasrallah, M.M., Anderson, H.U., Sparlin, D.M., and Sehlin, S.R. (1995) Structure and electrical properties of $La_{1-x}Sr_xCo_{1-y}Fe_yO_3$. Part 1. The system $La_{0.8}Sr_{0.2}Co_{1-y}Fe_yO_3$. Solid State Ionics, 76, 259-271.

[6] Sekido, S., Tachibana, H., Yamamura, Y., and Kambara, T. (1990) Electric–ionic conductivity in perovskite–type oxides, $Sr_xLa_{1-x}Co_{1-y}Fe_yO_{3-\delta}$. Solid State Ionics, 37, 253-259.

[7] Wang, S., Katsuki, M., Dokiya, M., and Hashimoto, T. (2003) High temperature properties of $La_{0.6}Sr_{0.4}Co_{0.8}Fe_{0.2}O_{3-\delta}$ phase structure and electrical conductivity. Solid State Ionics, 159, 71-78.

[8] Greenblatt, M. (1997) Ruddlesden-Popper $Ln_{n+1}Ni_nO_{3n+1}$ nickelates: Structure and properties. Solid State & Mater. Sci., 2, 174-183.

[9] Vashook, V.V., Yushkevich, I.I., Kokhanovsky, L.V., Makhnach, L.V., Tolochko, S.P., Kononyuk, I.F., Ullmann, H., and Altenburg, H. (1999) Composition and conductivity of some nickelates. Solid State Ionics, 119, 23-30.

[10] Tang, J.P., Dass, R.I., and Manthiram, A. (2000) Comparison of the crystal chemistry and electrical properties of $La_{2-x}A_xNiO_4$ (A = Ca, Sr, and Ba). Mater. Res. Bull., 35, 411-424.

[11] Hui, Z., Qiang, L., and LiPing, S. (2011) Ln_2MO_4 Cathode materials for solid oxide fuel cells. Sci. China Chem., 54, 898-910.

[12] Amow, G. and Skinner, S.J. (2006) Recent developments in Ruddlesden-Popper nickelate systems for solid oxide fuel cell cathodes. J. Solid State Electrochem., 10, 538-546.

[13] Routbort, J.L., Doshi, R., and Krumpelt, M. (1996) Oxygen tracer diffusion in $La_{1-x}Sr_xCoO_3$. Solid State Ionics, 90, 21-27.

[14] Fontaine, M.L., Laberty-Robert, C., Ansart, F., and Tailhades, P. (2006) Composition and porosity graded $La_{2-x}NiO_{4+\delta}$ ($x \geq 0$) interlayers for SOFC: control of the microstructure via a sol–gel Process. J. Power Source, 156, 33-38.

[15] Weng, X., Boldrin, P., Abrahams, I., Skinner, S.J., and Darr, J. A. (2007) Direct syntheses of mixed ion and electronic conductors $La_4Ni_3O_{10}$ and $La_3Ni_2O_7$ from nanosized coprecipitates. Chem. Mater., 19, 4382-4384

[16] Zhang, Z. and Greenblatt, M. (1995) Synthesis, structure and properties of $Ln_4Ni_3O_{10-\delta}$. J. Solid State Chem., 117, 236-246.

[17] Fuertes, V.C., Blanco, M.C., Franco, D.G., De Paoli, J.M., Sa´nchez, R.D., and Carbonio, R.E. (2011) Influence of the B-site ordering on the magnetic properties of the new $La_3Co_2MO_9$ double perovskites with M = Nb or Ta. Mater. Res. Bull., 46, 62-69.

[18] Nowick, A.S., Du, Y., and Liang, K.C. (1999) Some factors that determine proton conductivity in nonstoichiometric complex perovskites. Solid State Ionics, 125, 303-311.

[19] Nowick, A.S. and Liang, K.C. (2000) Effect of non-stoichiometry on the protonic and oxygen-ionic conductivity of $Sr_2(ScNb)O_6$: a complex perovskite. Solid State Ionics, 129, 201-207.

[20] Kim, J.-H. and Manthiram, A. (2009) Layered $NdBaCo_{2-x}Ni_xO_{5+\delta}$ perovskite oxides as cathodes for intermediate temperature solid oxide fuel cells. Electrochim. Acta, 54, 7551-7557.

[21] Hu, Y., Bogicevic, C., Bouffanais, Y., Giot, M., Hernandez, O., and Dezanneau, G. (2013) Synthesis, physical-chemical characterization and electrochemical performance of $GdBaCo_{2-x}Ni_xO_{5-\delta}$ (x = 0-0.8) as cathode materials for IT-SOFC application. J. Power Sources, 242, 50-56.

[22] Tao, S. and Irvine, J.T.S. (2002) Structure and properties of nonstoichiometric mixed perovskites $A_3B'_{1+x}B''_{2-x}O_{9-\delta}$. Solid State Ionics, 154-155, 659-667.

[23] Kudo, A., Kato, H., and Nakagawa, S. (2000) Water splitting into H_2 and O_2 on new $Sr_2M_2O_7$ (M = Nb and Ta) photocatalysts with layered perovskite structures: Factors affecting the photocatalytic activity. J. Phys. Chem. B, 104, 571-575.

[24] Lufaso, M.W. (2004) Crystal structures, modeling, and dielectric property relationships of 2:1 ordered $Ba_3MM'_2O_9$ (M = Mg, Ni, Zn; M′ = Nb, Ta) perovskites. Chem. Mater., 16, 2148-2156.

[25] Verma, V., Gairola, S.P., Pandey, V., Kotanala, R.K., and Su, H. (2008) Permeability of Nb and Ta doped lithium ferrite in high frequency range. Solid State Commun., 148, 117-121.

[26] Kammer, K. (2006) Studies of Fe–Co based perovskite cathodes. Solid State Ionics, 177, 1047-1051.

[27] Xu, G., Funahashi, R., Pu, Q., Liu, B., Tao, R., Wang, G., and Ding, Z. (2004) High–temperature transport properties of Nb and Ta substituted $CaMnO_3$ system. Solid State Ionics, 171, 147-151.

[28] Palanduz, C.A. and Smyth, D.M. (1999) The effect of cation place exchange on the electrical conductivity of $SrBi_2M_2O_9$ (M = Ta, Nb). J. Eur. Ceram. Soc., 19, 731-735.

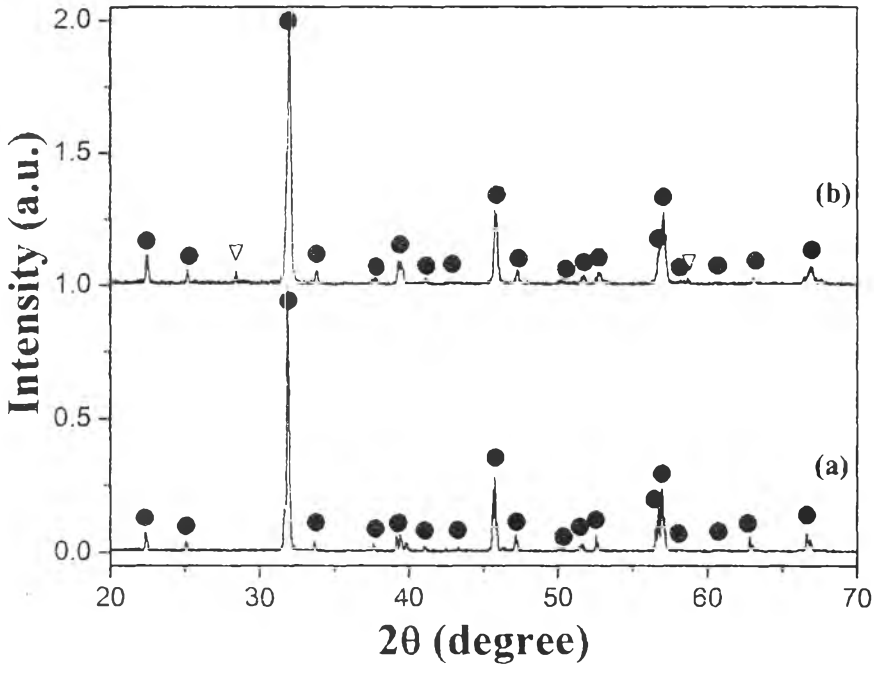

Figure 6.1 XRD patterns of $La_3Ni_2NbO_9$ samples prepared by (a) the solid state reaction and (b) the sol-gel process. (● = $La_2Mg_{1.33}Nb_{0.67}O_6$ and ∇ La_2O_3).

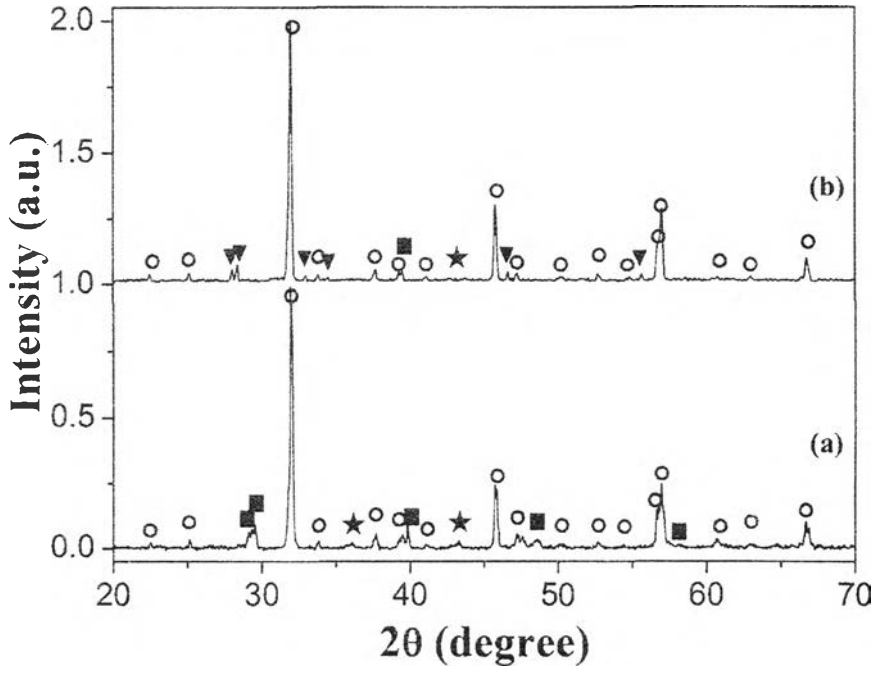

Figure 6.2 XRD patterns of $La_3Ni_2TaO_9$ samples prepared by (a) the solid state reaction and (b) the sol-gel process (○ $La_2Mg_{1.33}Ta_{0.67}O_6$, ▼ La_3TaO_7, ■ La_2O_3 and ★ NiO).

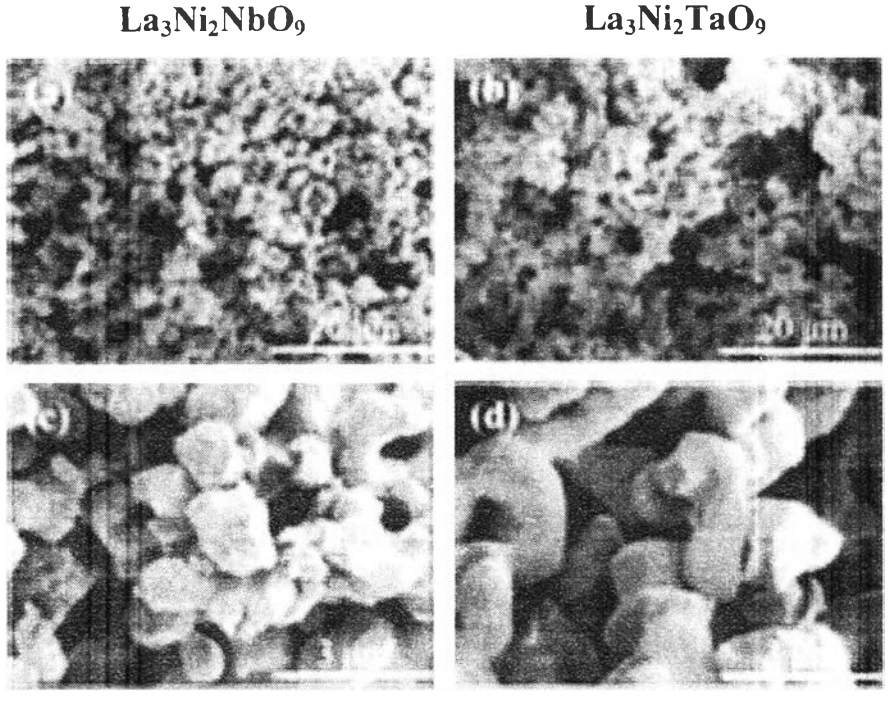

Figure 6.3 SEM images at different magnifications of the samples prepared by the solid state reaction after calcination at 1400°C for 24 h when $La_3Ni_2NbO_9$ is (a) and (c) and $La_3Ni_2TaO_9$ is (b) and (d).

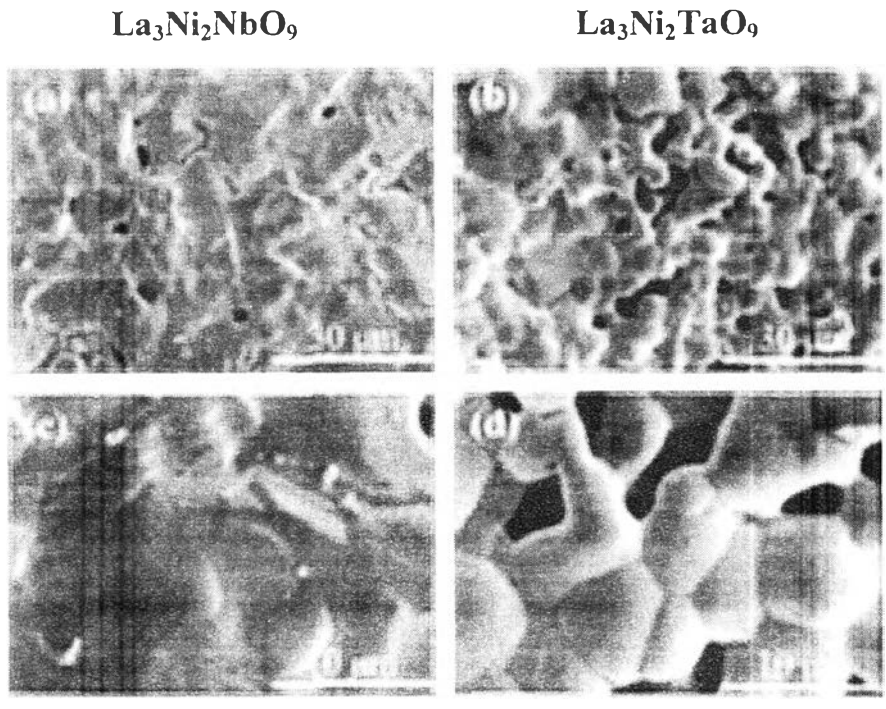

Figure 6.4 SEM images at different magnifications of the samples prepared by the solid state reaction after sintered at 1500°C for 24 h when $La_3Ni_2NbO_9$ is (a) and (c) and $La_3Ni_2TaO_9$ is (b) and (d).

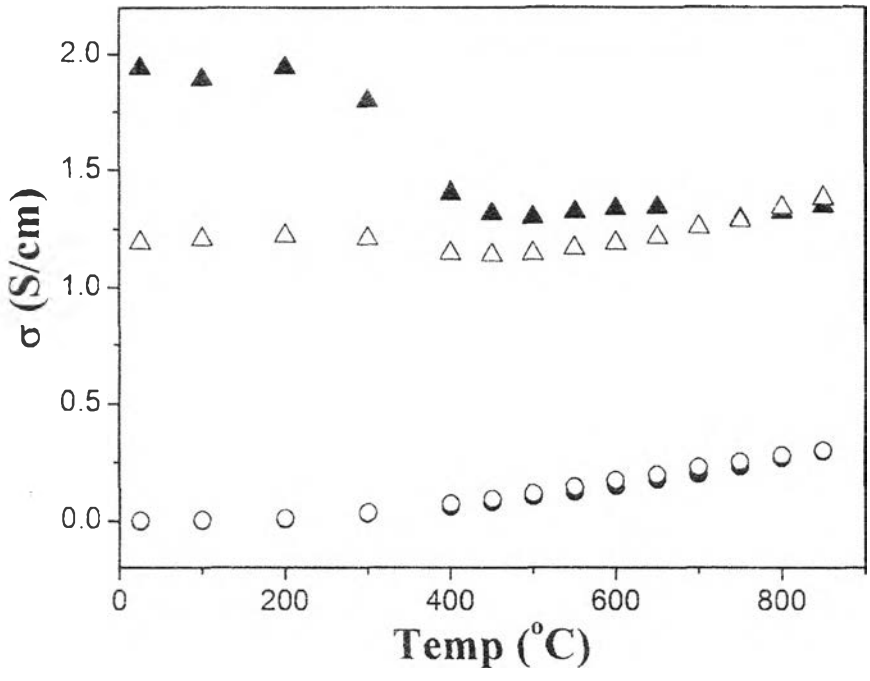

Figure 6.5 Electrical conductivity vs temperature plot of $La_3Ni_2NbO_9$ and $La_3Ni_2TaO_9$ samples prepared by the solid–state reaction measured in the temperature range (25°C-850°C) (● = $La_3Ni_2NbO_9$ and ▲= $La_3Ni_2TaO_9$ (closed symbols are values when heating up) and ○ = $La_3Ni_2NbO_9$ and Δ = $La_3Ni_2TaO_9$ (opened symbols when cooling down)).